SUPPLEMENTAL MATERIALS

High salt intake worsens aortic dissection in mice: involvement of IL-17A-dependent extracellular matrix metabolism

Norifumi Nishida, MD [1], Hiroki Aoki, MD, PhD [2], Satoko Ohno-Urabe, MD, PhD [1], Michihide Nishihara, MD, PhD [1], Aya Furusho, MD, PhD [1], Saki Hirakata, MD [1], Makiko Hayashi, MD [1], Sohei Ito, MD [1], Hiroshi Yamada, PhD [3], Yuichiro Hirata, MD, PhD [4], Hideo Yasukawa, MD, PhD [1], Tsutomu Imaizumi, MD, PhD [5], Hiroyuki Tanaka, MD, PhD [4], Yoshihiro Fukumoto, MD, PhD [1]

Affiliations

1. Division of Cardiovascular Medicine, Department of Internal Medicine, Kurume University School of Medicine, Kurume, Japan
2. Cardiovascular Research Institute, Kurume University, Kurume, Japan
3. Department of Biological Functions Engineering, Graduate School of Life Science and Systems Engineering, Kyushu Institute of Technology, Kitakyushu, Japan
4. Division of Cardiovascular Surgery, Department of Surgery, Kurume University School of Medicine, Kurume, Japan
5. International University of Health and Welfare, Fukuoka, Japan

EXPANDED METHODS

The data, analytical methods, and study materials will be available to other researchers for the purpose of reproducing the results or replicating the procedure as long as the situation allows. The transcriptome dataset has been deposited in Gene Expression Omnibus of the National Center for Biotechnology Information (accession # GSE116434). The study materials are commercially available except for human AAA tissue samples, which will not be publicly available. For the sources of animals, cell lines, and antibodies, please see the Major Resources Table.

Animal experiments

All animal protocols were approved by the Animal Experiments Review Boards of Kurume University. All mice were fed normal chow and allowed access to freely available drinking water unless otherwise stated. All of the animal experiments were carried out using male mice aged 11-14 weeks because AD predominantly affects men.[1] AD was induced by simultaneous administration of BAPN (150 mg/kg/day) and AngII (1000 ng/kg/min) using osmotic minipumps (Alzet model 1002). Two pumps, one for BAPN and another for AngII, were implanted while the mice were under anesthesia with 2% isoflurane. The mice were killed by pentobarbital overdose at the indicated time points to collect blood and tissue samples (Supplemental Fig. S1). The aortic tissue was excised either immediately for protein and mRNA expression analysis, or after perfusion and fixation with 4% paraformaldehyde in phosphate-buffered saline (PBS) at physiological pressure for histological analysis. To analyze protein and mRNA expression, a 10-mm length of aorta was excised above the branching point of the right renal artery, quickly frozen in liquid nitrogen, and stored at -80˚C until sample extraction.

High salt challenge and genetic modification of mice

High salt challenge was achieved by substituting 1% NaCl for drinking water for the indicated time period. We used mice with a genetic deletion of *Il17a* (IL17-KO) [2] backcrossed with C57BL/6J mice for more than eight generations to investigate the role of IL-17 in AD pathogenesis. Wild-type (WT) C57BL/6J mice (Charles River

Laboratories, Japan) served as a control.

Quantitative assessment of AD lesions

From a clinical perspective, the severity of AD is assessed by the extent and location of aortic wall destruction, which affects life-threatening complications, such as rupture, cardiac tamponade, and distal ischemia.[3, 4] A detailed three-dimensional analysis of our mouse model by propagation-based phase-contrast synchrotron imaging indicated progressive disruption of multiple medial layers, a hallmark of AD, associated with the formation of intramural hematoma and increased aortic diameter.[5] Visually, the AD lesions with a hematoma had an increased diameter. Accordingly, the lesions with aortic wall destruction due to AD were defined in this study by a diameter at least 1.5-fold greater than the reference diameter. The normal aortic diameter differs in different segments of the aorta; therefore, we divided the aorta into four segments (Supplemental Fig. S2): the aortic arch, from the aortic root to just distal of the left subclavian artery; the descending thoracic aorta to just proximal of the celiac trunk; the suprarenal aorta to just proximal of the left renal artery; and the infrarenal aorta to the iliac bifurcation. The reference diameter was measured at the most distal part of each segment in eight mice of the relevant genotype and the mean value used. We also characterized the severity of AD by the rate of thoracic or abdominal aortic rupture.

Expression analysis

To analyze protein expression, frozen aortic samples were pulverized using the SK mill (TOKKEN, Japan) and proteins extracted with RIPA buffer (Nacalai tesque #08714-04, Japan). After resolving the proteins using NuPAGE (Invitrogen), immunoblotting was performed with antibodies for phospho-Stat3 (P-Tyr705, Cell Signaling Technology #9145), NFκB (Cell Signaling Technology #8242), phospho-NFκB (P-Ser311, Enogene #E011260-1), Smad2 (Cell Signaling Technology #5339), phoshpo-Smad2 (Ser465/467, Cell Signaling Technology #3108), Smad3 (Abcam #ab40854), phospho-Smad3 (Ser423/Ser425, Abcam #ab52903), Smad4 (Abcam #ab195554), phospho-Jnk (Thr183/Tyr185, Cell Signaling Technology #4671), Smad7 (Abcam #ab190987), SM2 (Yamasa #7601), non-muscle myosin IIB (SMemb, Abcam #ab684), vimentin (Abcam

#ab92547), calponin-1 (Abcam #ab46794), glyceraldehyde-3-phosphate dehydrogenase (GAPDH, Millipore #MAB374), and β-actin (Cell Signaling Technology #4970). Plasma levels of IL-17A were measured using a bead-based assay (Bio-Plex, Bio-Rad #171-G5013M) at the indicated time points. To analyze mRNA expression, we isolated total RNA from the same part of the aorta as the protein expression analysis using the RNeasy kit (Qiagen). We performed transcriptome analyses using the SurePrint G3 Mouse Gene Expression v2 8x60K Microarray Kit (Agilent). The dataset has been deposited to the Gene Expression Omnibus of the National Center for Biotechnology Information (accession # GSE116434). Biological process-focused gene enrichment analysis was performed using the Database for Annotation, Visualization, and Integrated Discovery (DAVID, https://david.ncifcrf.gov/)[6] with the Gene Ontology terms set to GOTERM_BP_FAT. Expression of the indicated genes were measured by quantitative reverse transcription-polymerase chain reaction (qRT-PCR) using commercially available probes (Qiagen).

Histological analysis

We performed Elastica van Gieson (EVG) or hematoxylin–eosin (HE) staining on 5-μm paraffin-embedded sections of aortic tissue. Imaging cytometric analysis of mouse aortas was performed using an ArrayScan XTI (Thermo Fisher Scientific). Two aortic tissue sections were obtained from each mouse in the WT (n=8) and IL-17KO (n=8) groups. The tissue sections were stained for phospho-Smad2 (Ser465/467, Cell Signaling Technology #4671) using the TSA labeling kit and Alexa Fluor 488 tyramide (Invitrogen #T-20922). The tissue sections were also stained for smooth muscle α-actin (SMA, Sigma-Aldrich #A5228) with Cy3-conjugated secondary antibody (Jackson ImmunoResearch #715-165-151), and the nuclei with DAPI (4',6-diamidino-2-phenylindole) in the mounting media (VECTASHIELD Hardset Antifade Mounting Medium with DAPI, Vector Laboratories #H-1500). Microscopic images were obtained using a computerized bright field/wide field fluorescence microscope (BZ-9000, Keyence, Japan) or laser scanning confocal microscope (FV-1000, Olympus, Japan). The cytometric data obtained with the ArrayScan XTI were analyzed using FlowJo 10 software (FlowJo).

Collagen deposition in aortic walls

For the histological analysis of collagen deposition, we stained the aortic tissue sections with picrosirius red. We obtained the tissue sections from descending thoracic aorta just distal to left subclavian artery, because this segment is frequently affected by AD and was used for the measurement of mechanical properties. Bright field and polarized light-illuminated histological images were used. The area between the innermost and outermost elastic lamellae, the aortic media, was traced manually on the bright field images. The collagen deposition area, determined by picrosirius red staining in the media or adventitia, and the medial area were measured using ImagePro Plus software (version 7.0.1, Media Cybernetics). The percent collagen deposition in the media or adventitia was calculated by dividing the picrosirius red–positive area by the medial area of the corresponding section.

Stiffness of the aortic walls

To measure the mechanical properties of the aorta, we used a device that we developed (Muromachi Kikai, Japan). Briefly, we cut aortic rings with a width of 0.6 mm from the descending thoracic aorta (Supplemental Fig. S3), as this segment is frequently affected by AD. Also, this segment is devoid of major aortic branches that affect the mechanical properties. For the same reason, aortic rings with intercostal arteries were excluded from the measurement. During the preparation of the aortic rings, the ventral side of the aorta was painted with dye to identify the orientation. The aortic ring was immersed in calcium-free PBS containing 10 mM 2,3-butanedione monoxim to suppress smooth muscle cell (SMC) contraction [7] and mounted on two tungsten rods (0.25 mm diameter) oriented to the lateral sides of the aorta. The tungsten rods were pulled apart at a speed of 0.1 mm/sec until the aortic ring was broken. This was recorded by video and the passive force documented. Because we used aortic rings, rather than linearized strips, half of the measured force reflects the wall stress. We simultaneously measured the force development and the displacement of the aortic ring from the maximal length without force development. As an index of aortic wall stiffness, we calculated the mean force/displacement ratio from 0 mN to 5 mN, which corresponds to approximately 0

mmHg to 80 mmHg of blood pressure provided that the aortic ring diameter, the wall thickness, and the width are 0.8 mm, 0.075 mm, and 0.6 mm, respectively.

Cell culture experiments

Mouse aortic SMCs (#JCRB0150) were obtained from the National Institutes of Biomedical Innovation, Health and Nutrition (Tokyo, Japan) and maintained in Dulbecco's modified Eagle's medium (DMEM) with high glucose and fetal bovine serum (FBS). Confluent SMCs were serum-starved for 24 hours before starting the experiments. Serum-starved SMCs were stimulated with or without 25 ng/mL recombinant mouse IL-17A (R&D Systems, Minneapolis, MN, USA) for 24 hours, followed by 10 ng/mL recombinant mouse TGFβ1 (R&D Systems) for 1 hour. Cellular proteins were solubilized in RIPA buffer and subjected to immunoblotting.

Data acquisition and statistical analysis

Animals were randomly assigned to the experimental groups. The data were acquired by researchers or technicians who were blinded to the genetic modification and experimental intervention of the mice. All data are expressed as means ± standard errors. Statistical analyses were performed with GraphPad PRISM 5 (GraphPad Software). When the data passed the D'Agostino and Pearson normality test and Bartlett's test for equal variances, we performed an unpaired t-test for the two experimental groups or one-way analysis of variance to compare three or more groups, followed by Bonferroni's multiple comparison correction. For non-normal data distributions, we performed the Mann-Whitney U-test for two experimental groups, or Kruskal–Wallis test followed by Dunn's multiple comparison test for three or more groups. Significance was indicated by a two-sided $p<0.05$.

References for Expanded Methods

1. Nienaber CA, Fattori R, Mehta RH, Richartz BM, Evangelista A, Petzsch M, Cooper JV, Januzzi JL, Ince H, Sechtem U, Bossone E, Fang J, Smith DE, Isselbacher EM, Pape LA, Eagle KA, International Registry of Acute Aortic D. Gender-related differences in acute aortic dissection. *Circulation*. 2004;109:3014-

3021

2. Ishigame H, Kakuta S, Nagai T, Kadoki M, Nambu A, Komiyama Y, Fujikado N, Tanahashi Y, Akitsu A, Kotaki H, Sudo K, Nakae S, Sasakawa C, Iwakura Y. Differential roles of interleukin-17A and -17F in host defense against mucoepithelial bacterial infection and allergic responses. *Immunity*. 2009;30:108-119
3. Hiratzka LF, Bakris GL, Beckman JA, Bersin RM, Carr VF, Casey DE, Jr., Eagle KA, Hermann LK, Isselbacher EM, Kazerooni EA, Kouchoukos NT, Lytle BW, Milewicz DM, Reich DL, Sen S, Shinn JA, Svensson LG, Williams DM, American College of Cardiology Foundation/American Heart Association Task Force on Practice G, American Association for Thoracic S, American College of R, American Stroke A, Society of Cardiovascular A, Society for Cardiovascular A, Interventions, Society of Interventional R, Society of Thoracic S, Society for Vascular M. 2010 ACCF/AHA/AATS/ACR/ASA/SCA/SCAI/SIR/STS/SVM Guidelines for the diagnosis and management of patients with thoracic aortic disease. *J Am Coll Cardiol*. 2010;55:e27-e129
4. Cronenwett JL, Johnston KW. *Vascular Surgery*. Philadelphia: Elsevier Health Sciences; 2014.
5. Logghe G, Trachet B, Aslanidou L, Villaneuva-Perez P, De Backer J, Stergiopulos N, Stampanoni M, Aoki H, Segers P. Propagation-based phase-contrast synchrotron imaging of aortic dissection in mice: from individual elastic lamella to 3D analysis. *Sci Rep*. 2018;8:2223
6. Huang da W, Sherman BT, Lempicki RA. Systematic and integrative analysis of large gene lists using DAVID bioinformatics resources. *Nat Protoc*. 2009;4:44-57
7. Waurick R, Knapp J, Van Aken H, Boknik P, Neumann J, Schmitz W. Effect of 2,3-butanedione monoxime on force of contraction and protein phosphorylation in bovine smooth muscle. *Naunyn Schmiedebergs Arch Pharmacol*. 1999;359:484-492

Major Resources Tables

Animals (in vivo studies)

Species	Vendor or Source	Background Strain	Sex
Mouse	Tokyo University of Science, Center for Animal Disease Models	C57BL/6J	Male

Animal breeding

	Species	Vendor or Source	Background Strain	Other Information
Parent - Male	Mouse	Tokyo University of Science, Center for Animal Disease Models	C57BL/6J	*Il17a* deleted
Parent - Female	Mouse	Tokyo University of Science, Center for Animal Disease Models	C57BL/6J	*Il17a* deleted

Antibodies

Target antigen	Vendor	Catalog #	Working concentration (μg/mL)	Applications
β-actin	Cell Signaling Technology (CST)	#4970	0.05	WB
Calponin 1	Abcam	#ab46794	0.02	WB
GAPDH	Millipore	#MAB374	0.2	WB
NFkB	CST	#8242	1	WB
P-Jnk	CST	#4671	0.9	WB
P-NFkB	Enogene	#E011260-1	1	WB
P-Smad2	CST	#3108	0.05	WB

Antibodies (cont'd)

Target antigen	Vendor	Catalog #	Working concentration (µg/mL)	Applications
P-Smad3	Abcam	#ab52903	0.25	WB
P-Stat3	CST	#9145	0.5	WB
SM2	Yamasa	#7601	1:400, ascites (antibody concentration undetermined)	WB
Smad2	CST	#5339	0.28	WB
Smad3	Abcam	#ab40854	1	WB
Smad4	Abcam	#ab195554	0.1	WB
Smad7	Abcam	#ab190987	0.5	WB
SMemb	Abcam	#ab684	1:1000, ascites (antibody concentration undetermined)	WB
Vimentin	Abcam	#ab92547	0.25	WB
Mouse IgG	Jackson ImmunoResearch	#715-165-151	7.5	IF, Cy3-conjugated donkey anti-mouse IgG antibody
pSmad2	ThermoFisher	#44-244G	2.0	IF
Rabbit IgG isotype control	Abcam	#ab172730	2.0	IF
Smooth muscle α-actin	Sigma-Aldrich	#A5228	0.2	IF
Mouse IgG2a isotype control	Sigma-Aldrich	#MABC004	0.2	IF

Cultured Cells

Name	Vendor or Source	Sex
Aortic smooth muscle cells, #JCRB0150	The National Institutes of Biomedical Innovation, Health and Nutrition (Tokyo, Japan)	Unknown

SUPPLEMENTAL FIGURES

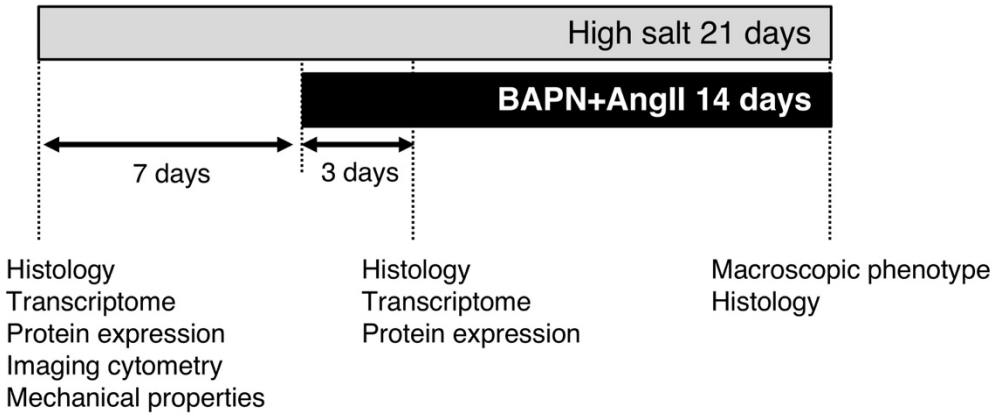

Supplemental Figure S1. Protocol for animal experiments.

The diagram shows the protocol for animal experiments. High salt condition (1% NaCl in drinking water) was maintained for 7 days before and throughout the AD-induction period with BAPN+AngII. Histological and expression analyses were performed 3 days after starting BAPN+AngII when visible AD was not observed. Macroscopic phenotype and histological analyses were performed at the end of 14 days of BAPN+AngII with or without high salt challenge.

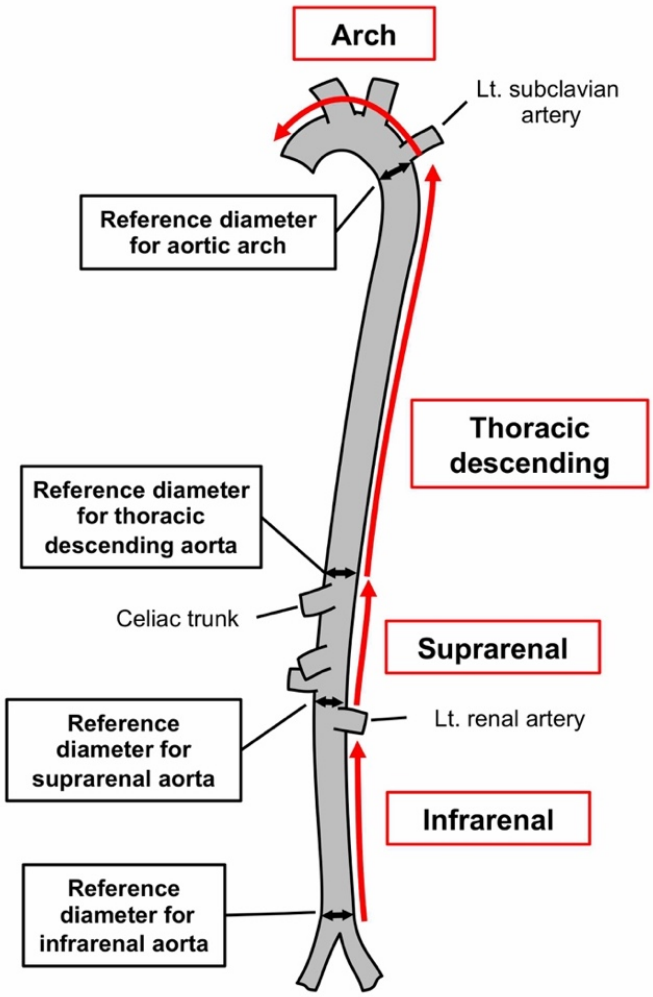

Supplemental Figure S2. Regional assessment of aortic wall destruction in the AD model.

The diagram shows the aortic segments (red arrows) and corresponding reference diameters at the distal site of each segment (black double arrows). The lesion length with aortic wall destruction due to AD was measured in four segments: the arch, thoracic descending, suprarenal, and infrarenal. In this study, a lesion with aortic wall destruction due to AD was defined by an at least 1.5-fold increased diameter compared to the reference diameter in each segment. The reference diameters were measured in eight mice of the relevant genotype and the mean values used.

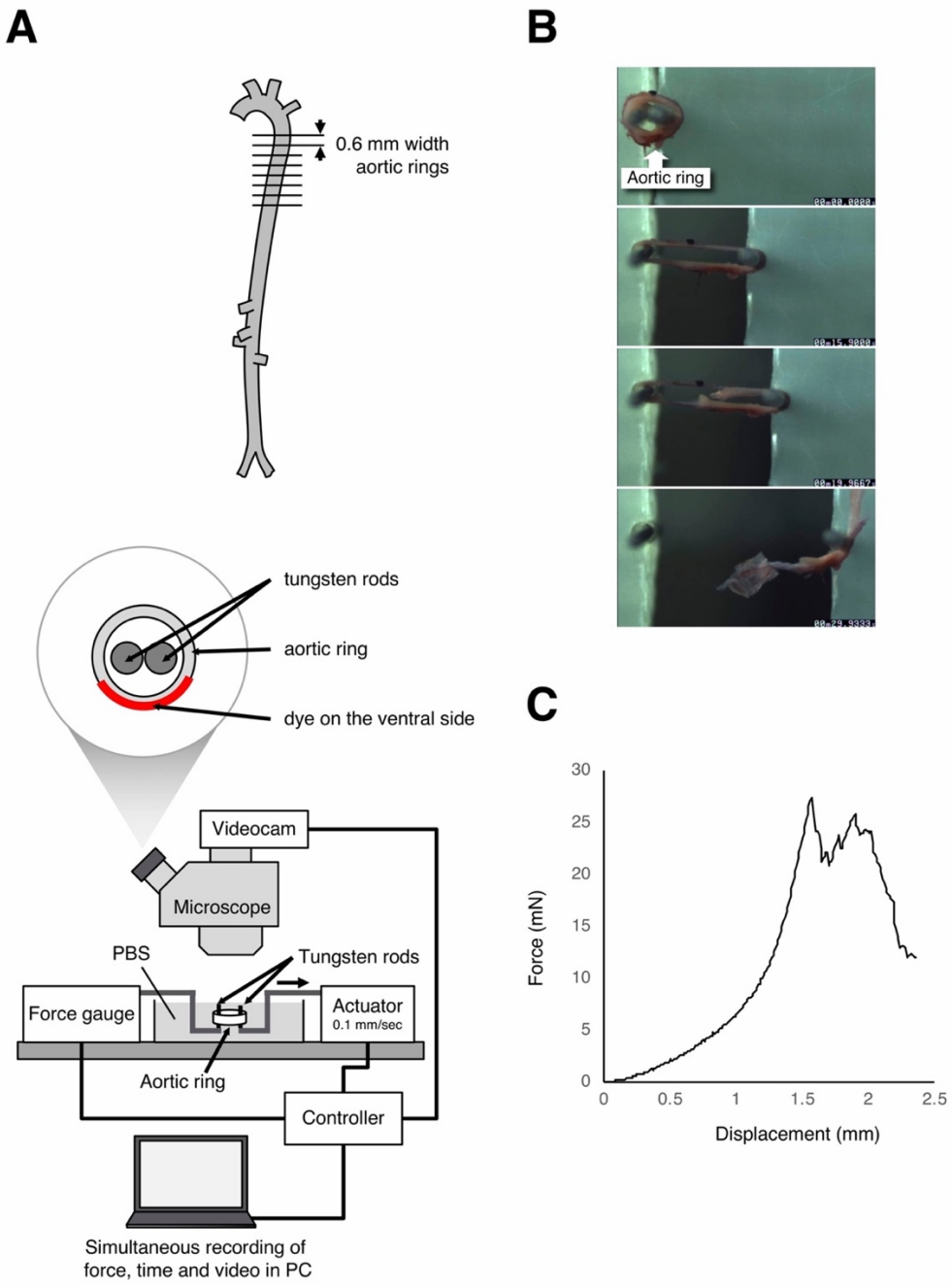

Supplemental Figure S3. Measurement of the biomechanical properties of the aortic wall.

(A) Diagrams of the procurement of aortic rings from the descending thoracic aorta (top) and the device for measuring the force-displacement relationship of the aortic rings (bottom). (B, C) A representative video recording (B) and force-displacement curve (C).

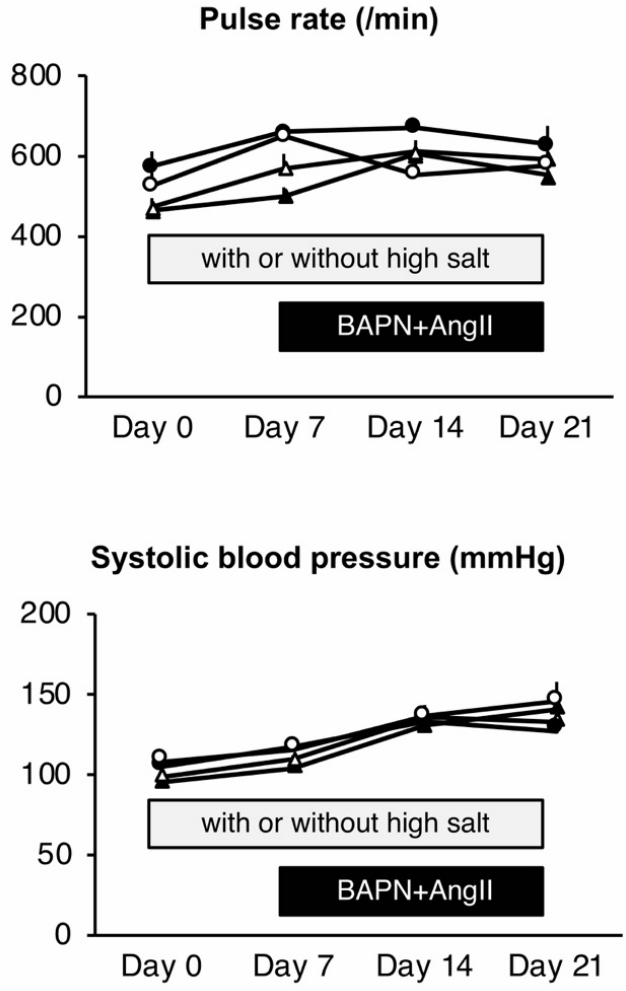

Supplemental Figure S4. Hemodynamic parameters in the AD model.

Pulse rate and systolic blood pressure in the AD model with (High salt, closed symbols) or without high salt (Normal salt, open symbols) intake in wild-type (circles) and IL-17KO (triangles) mice. Data represent the mean ± standard error for 8–12 mice in each group.

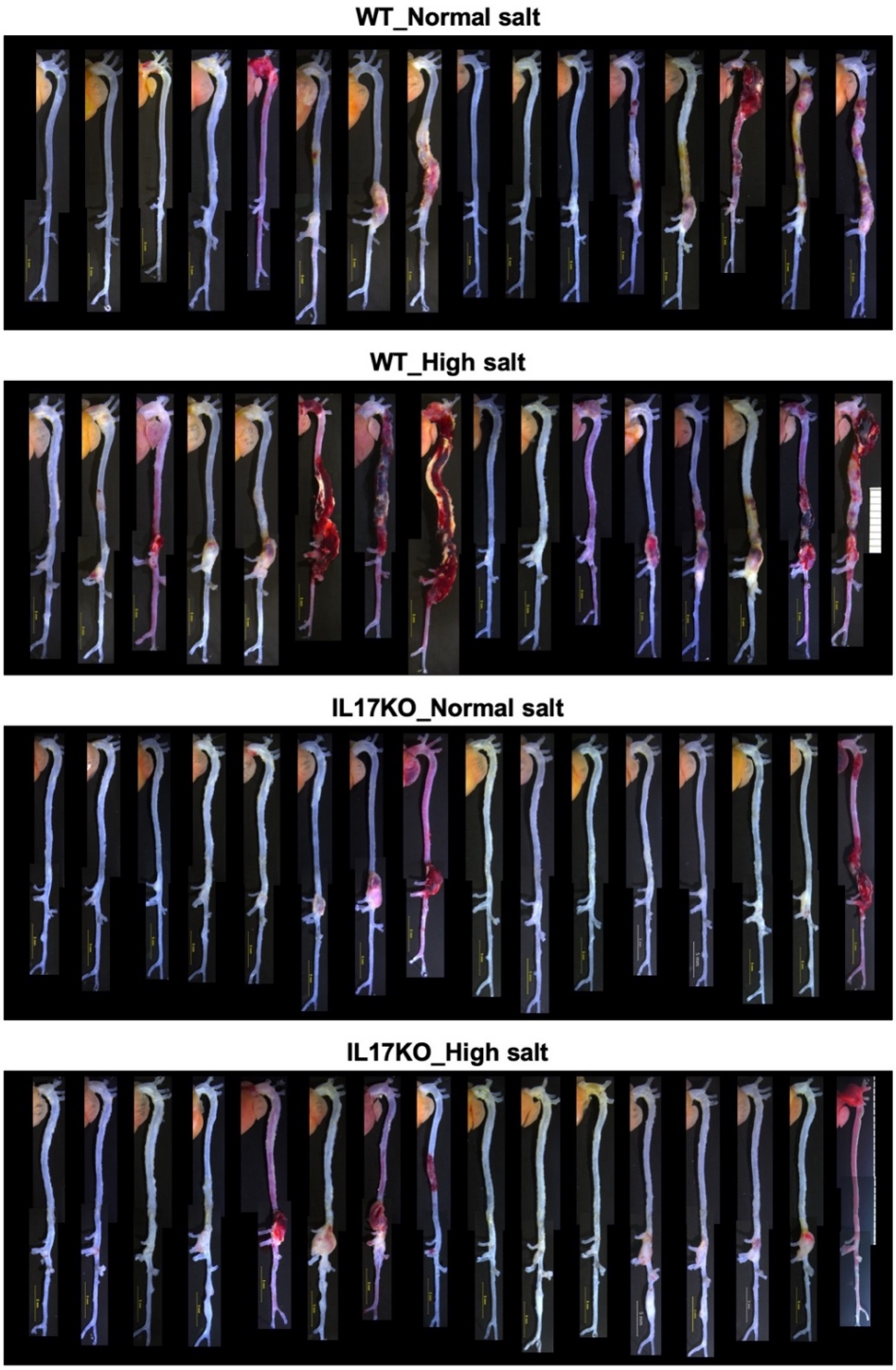

Supplemental Figure S5. Macroscopic images of mouse AD model

Macroscopic images are shown for aortas of wild type (WT) and IL-17KO mice 14 days after starting BAPN+AngII infusion with (High salt) and without (Normal salt) high salt challenge.

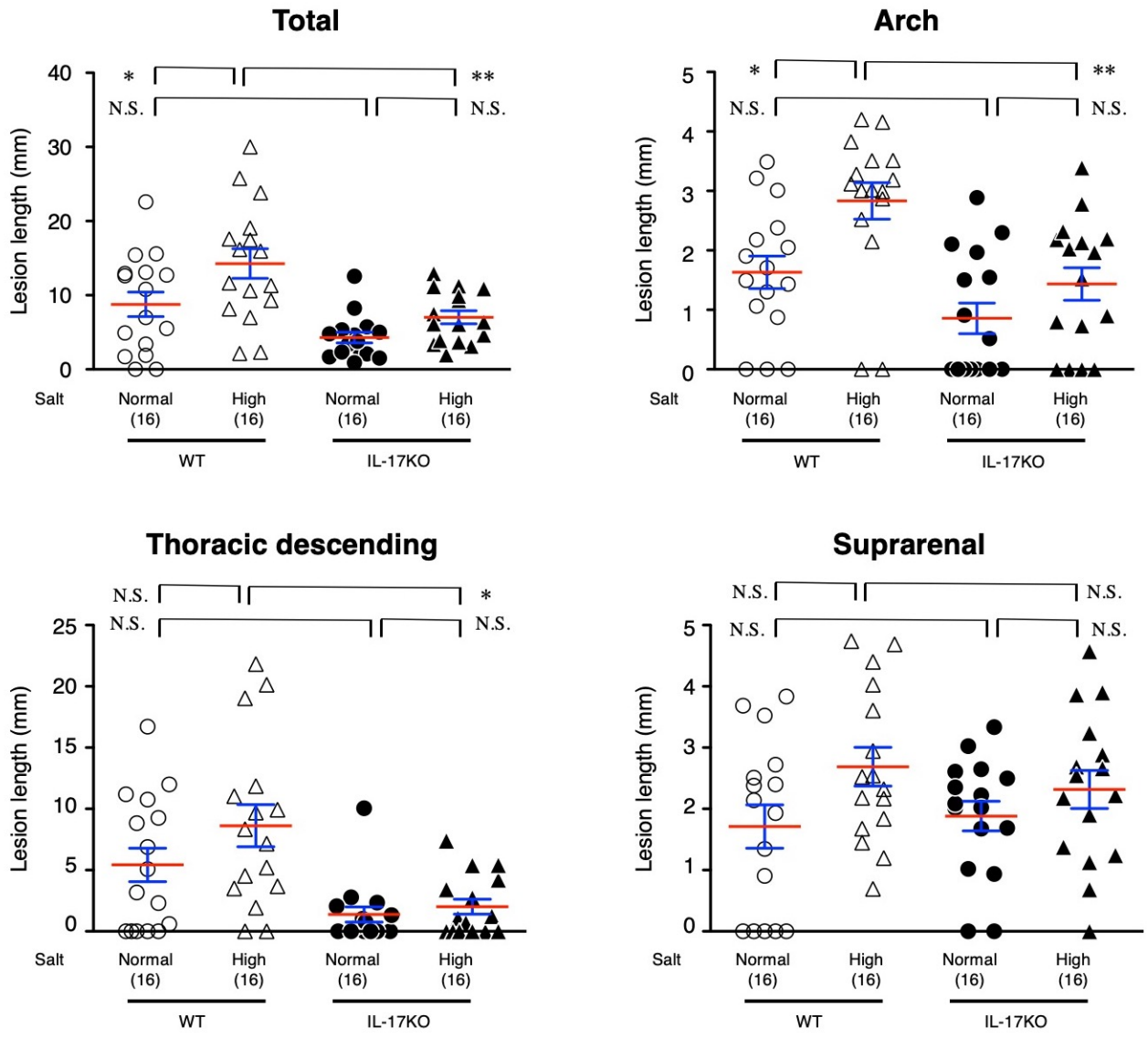

Supplemental Figure S6. AD lesion length in each aortic segment and lesion scores.

The AD lesion lengths are shown for individual aortic segments. The data were obtained from the same set of experiments as shown in Figure 2B. Data are presented as the mean (red lines) ± standard error (blue lines) of 16 mice in each experimental group; N.S., not significant, * $p < 0.05$, ** $p < 0.01$.

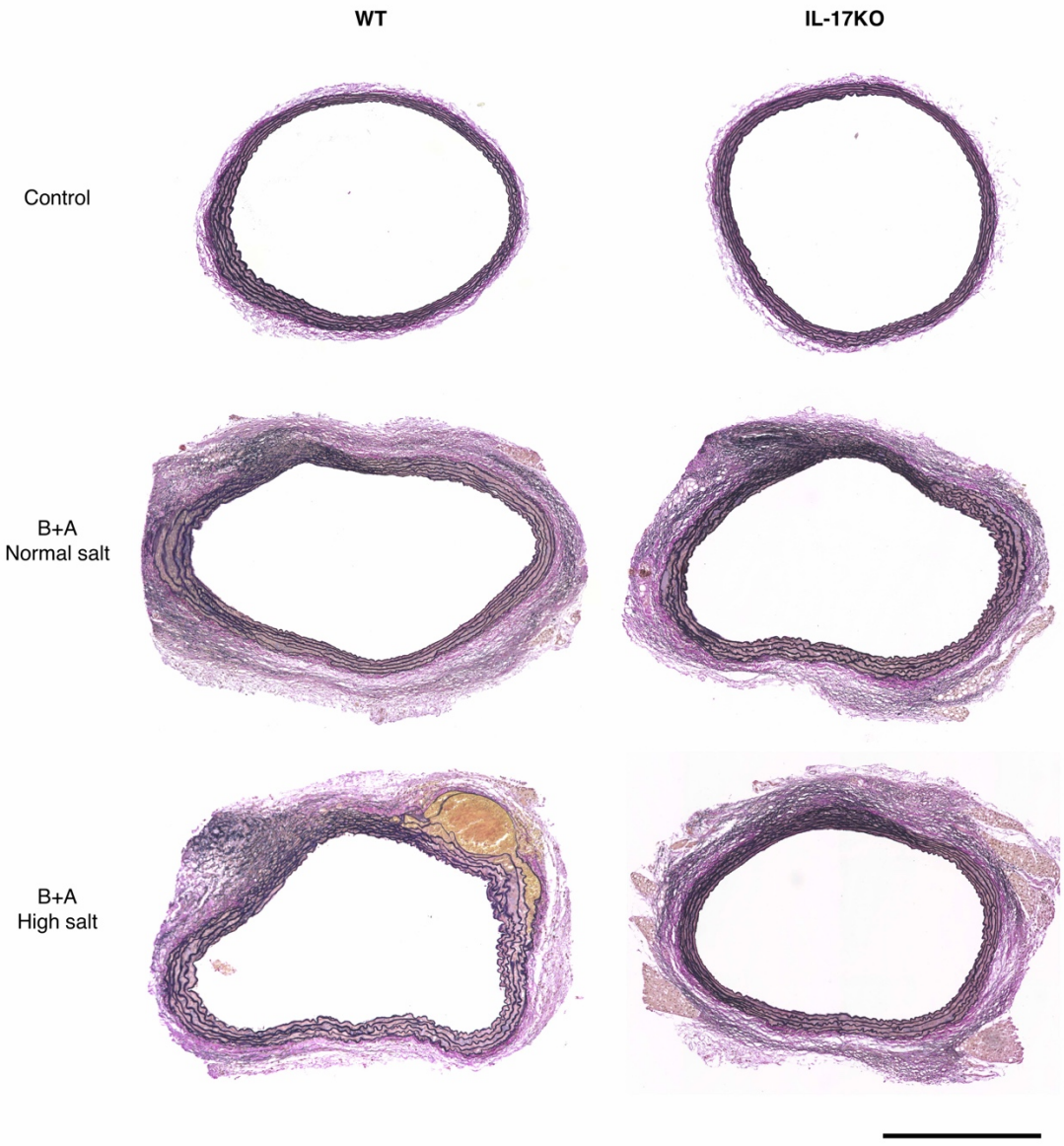

Supplemental Figure S7. Histology of the AD model induced by BAPN+AngII

Representative histochemical analysis with hematoxylin–eosin (HE) and Elastica van Gieson (EVG) stains are shown for aortic samples from WT and IL-17KO mice with or without BAPN+AngII (B+A) and high salt challenge. Scale bar = 500 μm.

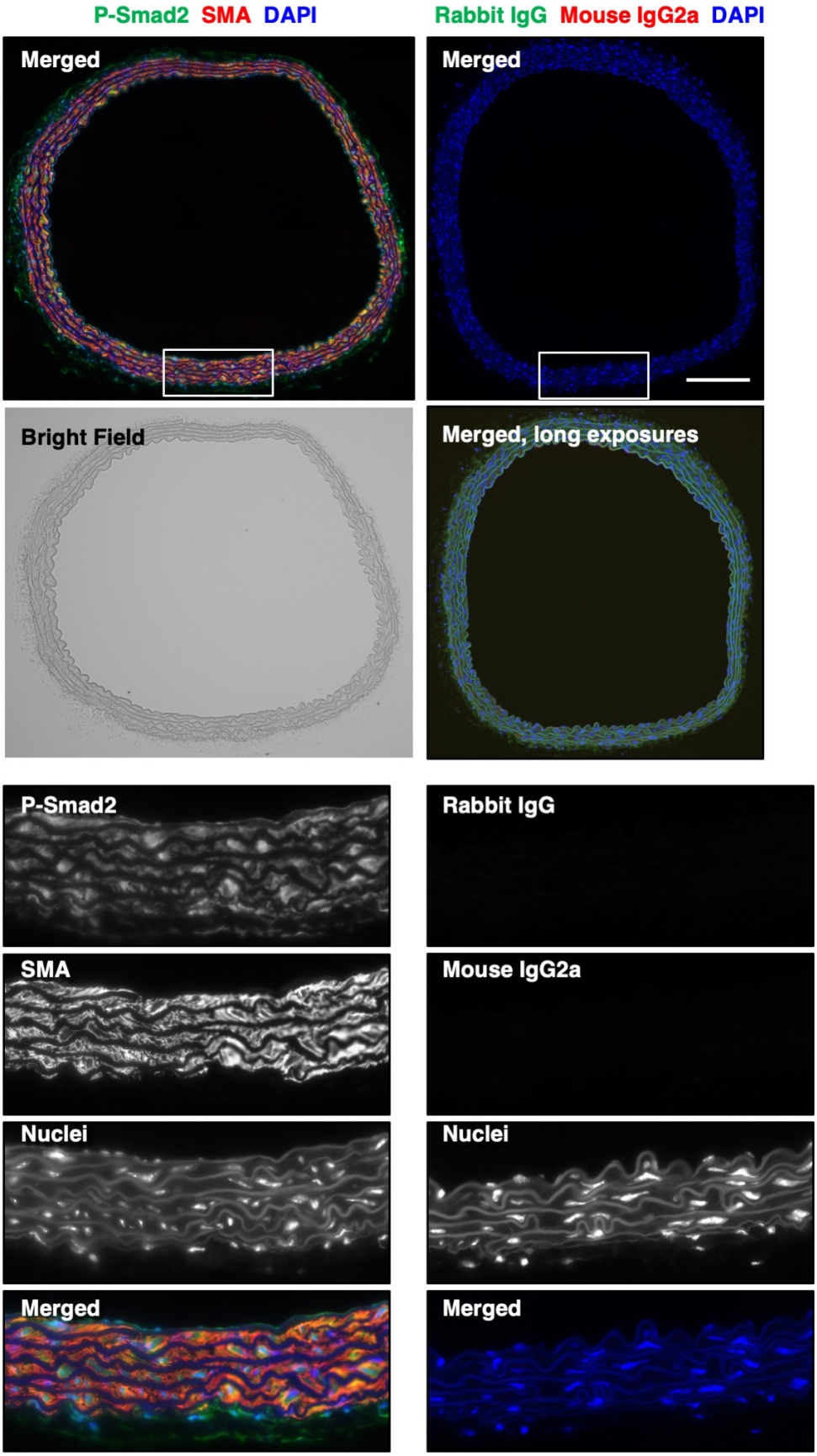
P-Smad2 SMA DAPI
Rabbit IgG Mouse IgG2a DAPI
Merged
Merged
Bright Field
Merged, long exposures
P-Smad2
Rabbit IgG
SMA
Mouse IgG2a
Nuclei
Nuclei
Merged
Merged

Supplemental Figure S8. Immunofluorescent staining of P-Smad2 and SMA. Left, Representative images are shown for immunofluorescent staining of phospho-Smad2 (P-Smad2), smooth muscle α-actin (SMA), and nuclei (by DAPI) in aortas. Right, Images of the negative control in which the sample was processed with isotype control antibodies corresponding to P-Smad (rabbit IgG) and SMA (mouse IgG2a) antibodies. The bottom panels show the enlarged images for the area indicated by the rectangles in the top panels. The short exposure of the aortic tissue treated with the isotype control antibodies exibits only DAPI fluorescence, and the long exposure image exhibits DAPI fluorescence and autofluorescence of elastic lamellae, demonstrating the specificity of P-Smad2 and SMA antibodies. Scale bar = 200 μm.

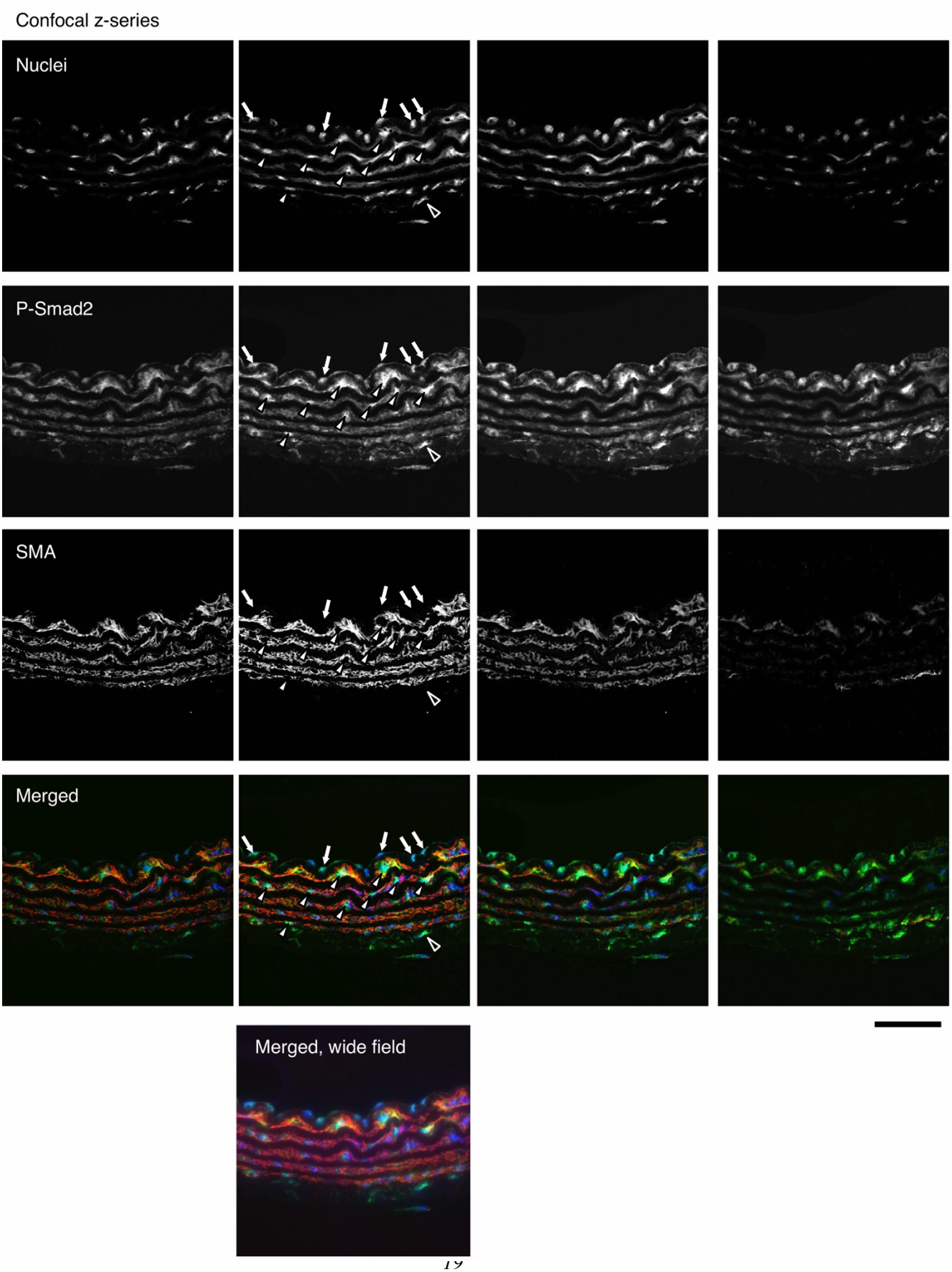
Confocal z-series
Nuclei
P-Smad2
SMA
Merged
Merged, wide field

Supplemental Figure S9. Confocal imaging of P-Smad2 and SMA.

Representative z-series images of optical sectioning by the laser confocal microscope for immunofluorescence staining of P-Smad2, smooth muscle α-actin (SMA), and nuclei. In merged images, nuclei, P-Smad2, and SMA are pseudo-colored blue, green, and red, respectively. White arrowheads, black arrowheads, and white arrows indicate SMA-positive cells, SMA-negative adventitial cells, and SMA-negative endothelial cells, respectively. An image from the conventional wide-field fluorescence microscope is also shown for the corresponding field. Scale bar = 50 μm. The z-series images show that the 5-μm sections contain a single layer of nuclei, and part of the P-Smad2-positive nuclei were surrounded by SMA, indicating that these cells were P-Smad2-positive smooth muscle cells.

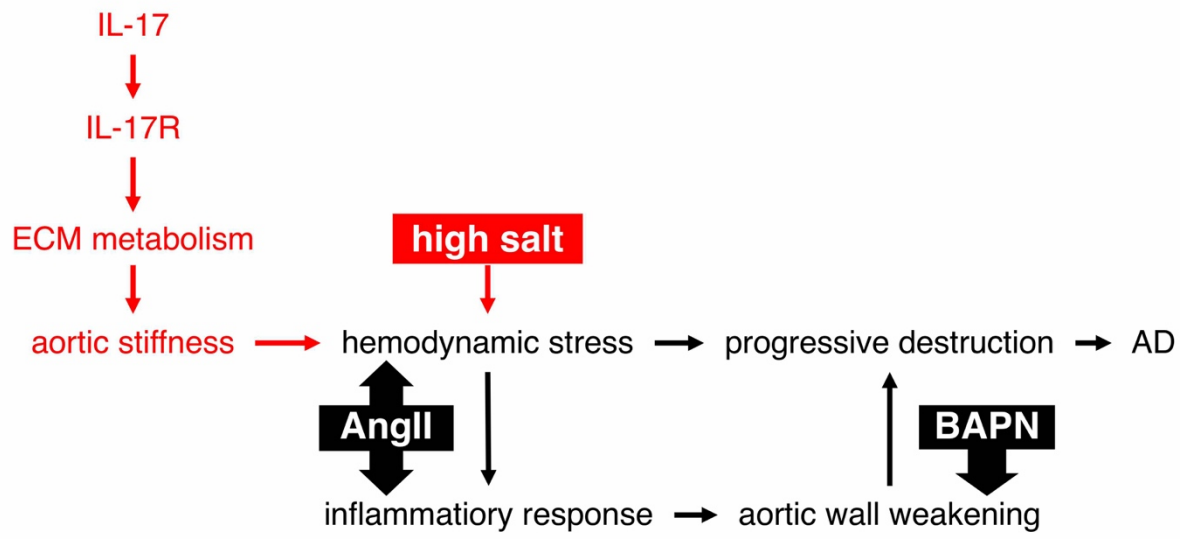

Supplemental Figure S10. Proposed mechanism for high salt and IL-17-dependent worsening of AD.

The AD model was created by continuous infusion of angiotensin II, which induces an inflammatory response and hemodynamic stress in aortic walls, and BAPN, which weakens aortic walls. IL-17 modulates ECM metabolism, causing aortic stiffness. High salt challenge augments the hemodynamic stress on stiff aorta, leading to a worsening of AD.

LEGENDS FOR SUPPLEMENTAL TABLES

Supplemental Table S1. Functional annotation of genes induced by BAPN+AngII.
Genes significantly induced by BAPN+AngII challenge (fold changes > 2.0 and $p < 0.05$) underwent functional annotation analysis using DAVID. The results correspond to the hierarchical clustering analysis and heatmap representation in Figure 1C.

Supplemental Table S2. Functional annotation of genes suppressed by BAPN+AngII.
Genes significantly suppressed by BAPN+AngII challenge (fold changes < 0.5 and $p < 0.05$) underwent functional annotation analysis using DAVID. The results correspond to the hierarchical clustering analysis and heatmap representation in Figure 1C.

Supplemental Table S3. Transcriptome of ECM-related genes.
The results of the transcriptome analysis are shown for genes with “extracellular matrix” in their Gene Ontology terms. The result corresponds to the hierarchical clustering analysis and heatmap representation in Figure 5.